Contents lists available at ScienceDirect

Nuclear Inst. and Methods in Physics Research, B

Behavior of Cu-Y$_2$O$_3$ and CuCrZr-Y$_2$O$_3$ composites before and after irradiation

R. Martins [a], F. Antão [a], J.B. Correia [b], E. Tejado [c], J. Pastor [c], A. Galatanu [d], P.A. Carvalho [e], E. Alves [a], M. Dias [a,*]

[a] Instituto de Plasmas e Fusão Nuclear, Instituto Superior Técnico, Universidade de Lisboa, Av. Rovisco Pais, 1049-001 Lisboa, Portugal
[b] LNEG, Laboratório Nacional de Energia e Geologia, Estrada do Paço do Lumiar, 1649-038 Lisboa, Portugal
[c] Departamento de Ciencia de Materiales-CIME, ETSI Caminos, Canales y Puertos, Universidad Politécnica de Madrid, E28015 Madrid, Spain
[d] National Institute of Materials Physics, Magurele 077125, Romania
[e] SINTEF Materials Physics, Forskningsveien 1, 0314 Oslo, Norway

ABSTRACT

The Cu-Y$_2$O$_3$ and CuCrZr-Y$_2$O$_3$ materials have been devised as thermal barriers in nuclear fusion reactors. It is expected that in the nuclear environments, the materials should be working on extreme conditions of irradiation. In this work the Cu-Y$_2$O$_3$ and CuCrZr-Y$_2$O$_3$ were prepared and then irradiated in order to understand the surface irradiation resistance of the material. The composites were prepared in a glove box and consolidated with spark plasma sintering. The microstructures revealed regions of Y$_2$O$_3$ dispersion and Y$_2$O$_3$ agglomerates both in the Cu matrix and in the CuCrZr. The irradiated samples did not show any surface modification indicating that the materials seem to be irradiation resistant in the present situation. The thermal conductivity values for all the samples measured are lower than pure Cu and higher than pure W, however are higher than those expected, and therefore, the application of these materials as thermal barriers is compromised.

1. Introduction

The high melting point, high sputtering threshold, and low tritium inventory turn tungsten into suitable material for plasma-facing and structural components in the first wall of nuclear fusion reactors. However, a major disadvantage of current tungsten grades is their relatively high ductile-to-brittle transition temperature [1]. Operation at higher temperatures is desirable to preserve W components' integrity. Due to its high conductivity, strength, and microstructural stability, a CuCrZr alloy has been selected as a heat sink material to remove heat from the plasma-facing components [2]. Since the service temperature of this material is relatively low [3], the operation at higher temperatures demands an interlayer between the plasma-facing W and the CuCrZr heat sink.

Moreover, the thermal expansion coefficient (CTE) of the W is smaller than the CuCrZr CTE, which can cause stresses at the interfaces [4]. This means, taking into account the significant temperature difference between W and CuCrZr optimum operating temperatures, the interlayer should have low thermal conductivities values of around 15 W/m/K and an elastic modulus of around 1 GPa for a 0.5 mm layer

thickness [5]. Several interface materials have been presented as candidates as interlayers, such as FeltMetal [4], W-Cu composite [6], and Cu reinforced with monofilament W (W$_f$-Cu) [7]. However, these materials do not fulfil all the requirements for application as thermal barriers.

A proposed strategy of this work is the production of oxide dispersion strengthened materials such as Cu-Y$_2$O$_3$ and CuCrZr-Y$_2$O$_3$ to be used as interlayers for nuclear fusion applications and its microstructural and thermo-physical characterization.

Oxide dispersion strengthened (ODS) alloys are an attractive option since they exhibit improved mechanical properties while maintaining excellent thermal properties [8–11]. It is established that the presence of such oxide particles can modify the thermal conductivity by forming scattering points for phonon conduction [12].

Moreover, some authors have shown that Cu-based composites (Cu-AlO as well as Cu-Y$_2$O$_3$ [13], and Cu-ZrO [14]) with high content of oxides 10–40 vol% and 50–90 vol% respectively, have excellent thermal properties presenting values of thermal conductivity between those expected as thermal barriers in a fusion reactor. Studies on copper-yttria ODS materials evidence an increase in yield strength of these materials

Table 1
Experimental conditions (temperature, pressure and holding time) for all compositions.

Samples (%v/v)	Experimental Conditions		
	Temperature (°C)	Pressure (MPa)	Holding time (min)
Cu-1Y$_2$O$_3$	800	57	5
Cu-5Y$_2$O$_3$	800	57	5
Cu-10Y$_2$O$_3$	780	57	8
CuCrZr-1Y$_2$O$_3$	800	57	5
CuCrZr-5Y$_2$O$_3$	800	57	5
CuCrZr-10Y$_2$O$_3$	780	57	8

Table 2
Experimental conditions of theoretical compositions (vol.%) for all compositions.

Compositions (vol.%)		Theoretical density (g/cm^3)
CuCrZr	99CuCrZr-1Y$_2$O$_3$	8.81
	95CuCrZr-5Y$_2$O$_3$	8.70
	90CuCrZr-10Y$_2$O$_3$	8.51
Cu	99CuCrZr-1Y$_2$O$_3$	8.91
	95CuCrZr-5Y$_2$O$_3$	8.75
	90CuCrZr-10Y$_2$O$_3$	8.55

due to the grain boundary strengthening as Cu-3Y$_2$O$_3$ and Cu-3CaO [15], Cu-0.42Y$_2$O$_3$ [16], Cu-10Y$_2$O$_3$ after ball milling process [17].

The use of heavy ion irradiation as a surrogate for studying the effects of neutron damage is a standard option, justified by studies of radiation-induced defect structures in ferritic/martensitic steels arising from heavy ions vs neutrons [18,19]. Despite expected differences in the damage nature and distribution produced by charged ions and neutrons, this type of analysis can indicate the radiation resistance potential of the alloys and their suitability as thermal barriers for fusion reactors.

Scanning electron microscopy (SEM) and transmission electron microscopy (TEM), both coupled with energy dispersive X-ray spectroscopy (EDS) were used to characterize the materials. Apparent density, (micro-) hardness, thermal diffusivity, and mechanical properties were also evaluated.

2. Experimental

Cu-Y$_2$O$_3$ and CuCrZr-Y$_2$O$_3$ powder mixtures with the volume fraction of 1, 5, and 10 of Y$_2$O$_3$ (v/v) % were produced by tubular blending for 1 h in N$_2$ atmosphere. The powder used were commercially pure Cu powder (irregular particles with size $<$ 37 μm) with 99.9% nominal purity, pure CuCrZr powder (irregular particles with size $<$ 45 μm with a nominal composition of 99Cu-0.85Cr-0.04Zr produced by atomization and pure Y$_2$O$_3$ (irregular particles with size $<$ 10 μm). The samples were consolidated by spark plasma sintering (SPS) processing in an FCT Systeme Gmbh sintering machine using a graphite molds. The samples were then sealed under vacuum (5x10^{-3} Pa), using temperatures ranging from 780 °C to 800 °C with pressures of 57 MPa with a holding time of 5–8 min then cooled to room temperature. The final discs produced have a volume of 0.53 cm^3 with an average weight of 4.5 g. The experimental conditions of the cycles for each sample are shown in Table 1.

The metallographic preparation involved grinding with SiC paper and polishing with 6 μm, 3 μm, and 1 μm grade diamond suspensions. The microstructures were investigated with secondary and back-scattered electron signals (SE and BSE, respectively) on polished as-sintered and irradiated surfaces using a JEOL JSM-7001F instrument operated at an accelerating voltage of 25 kV. Chemical information was obtained by X-ray energy dispersive spectroscopy (EDS). The apparent sample density was measured by the Archimedes method using a high-resolution balance. The theoretical densities are presented in Table 2.
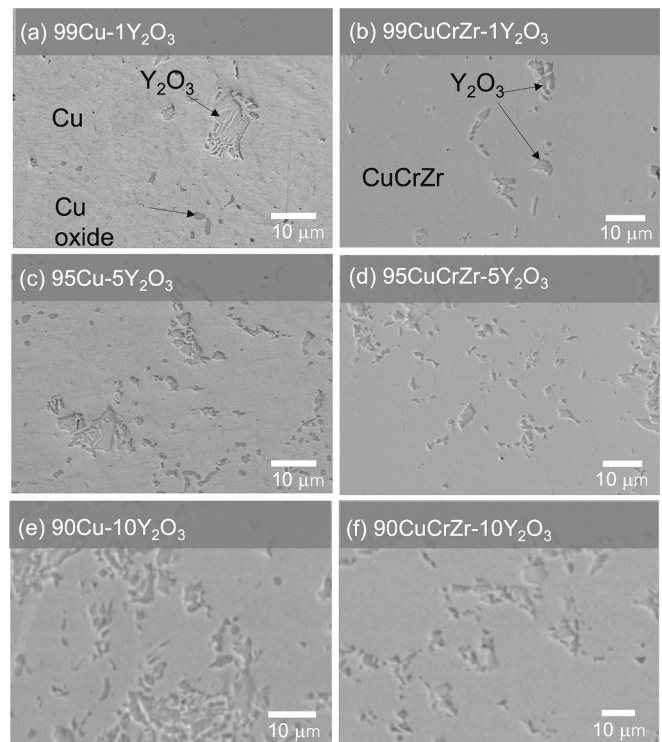
Fig. 1. Microstructures of Cu-Y$_2$O$_3$ samples with (a) 99Cu-1Y$_2$O$_3$, (c) 95Cu-5Y$_2$O$_3$ and (e) 90Cu- 10Y$_2$O$_3$ and for CuCrZr-Y$_2$O$_3$ with (b) 99CuCrZr-1Y$_2$O$_3$, (d) 95CuCrZr-5 Y$_2$O$_3$, (f) 90CuCrZr-10 Y$_2$O$_3$ compositions.

The thermal transport properties have been investigated using a Netzsch LFA457 Microflash up to 600 °C.

The effect of energetic particles (14 MeV neutrons) on the alloys was experimentally simulated using Ar$^+$ irradiation. The use of charged particles as a surrogate for neutron damage is an option, and this approach has recently been validated for comparing the radiation-induced defect structures in a ferritic/martensitic steel heavy ions and neutrons [18,19]. Several samples of CuCrFeTiV high entropy alloy were irradiated at room temperature with a 300 keV Ar$^+$ beam to a fluence of 1x10^{19} ions/cm^2. This fluence was set in order to cause damage levels amouting to ~100 dpa, as computed by the SRIM 2013 [16] and the irradiation depth is around 200 nm. Monte Carlo code for the number of defects caused by the moving argon ions. This is the average damage level expected from neutron irradiation during the foreseeable work cycle of a fusion reactor [20]. Several samples of the sintered 95Cu-5Y$_2$O$_3$ and 95CuCrZr-5Y$_2$O$_3$ were irradiated at room temperature with Ar$^+$ fluence of 1×10^{19} ions/cm^2.

Vickers micro-hardness was obtained by applying a load of 9.8 N for 15 s in an AKASHI MVK-EIII tester. Additionally, 95Cu-5Y$_2$O$_3$ samples, both irradiated and unirradiated, were tested using a MTS Nanoindenter XP in continuous stiffness mode (CSM) and a Berkovich indenter calibrated in fused silica following the Oliver-Pharr procedure [21]. Unlike the conventional quasistatic technique where a single depth is evaluated, CSM enables the determination of hardness and Young's modulus continuously throughout the indentation depth. This allows probing the relative effect of irradiation on the hardness at each depth. A maximum indentation depth of 2000 nm was set during the measurements, and for every material condition, 50 nanoindentation tests were conducted. Thus, quasi-static three-point bending (TPB) tests were performed using 16 mm loading span at a constant crosshead travel speed of 100 μm/min, to control the test process while obtaining accurate recording data quickly. Tests were performed on smooth bars of nominal dimensions $0,7 \times \sim 2.7 \times 19$ mm^3 machined by electro-discharge from the SPS disks. Prior to testing, samples surfaces were progresively grinded to 600
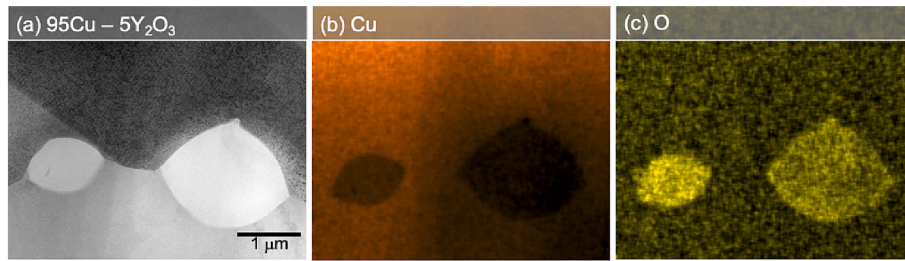
Fig. 2. EDS map in TEM of the (a) 95Cu-5Y$_2$O$_3$ sample and the corresponding EDS map with (b) Cu K-α and (c) O K-α X-ray lines.
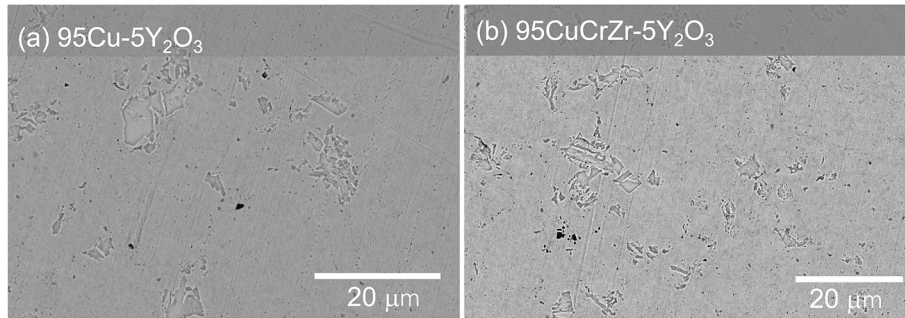

Fig. 3. Irradiated microstructures of the (a) 95Cu-5Y$_2$O$_3$ and (b) 95CuCrZr-5Y$_2$O$_3$ samples.
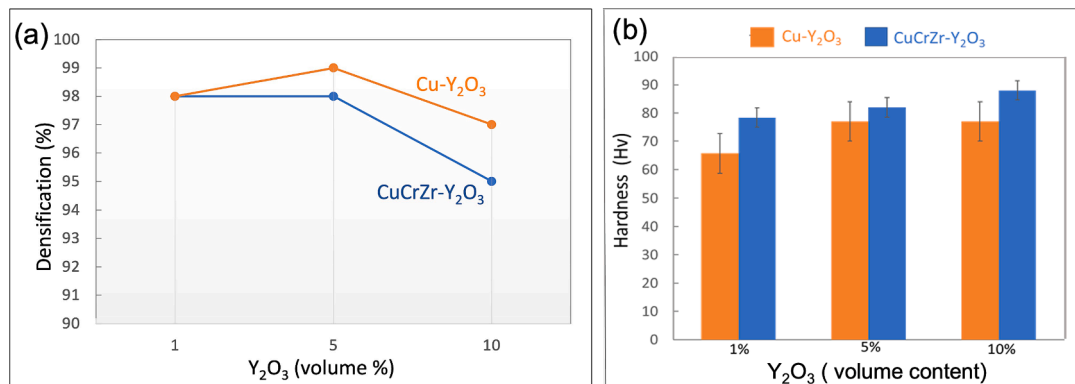

Fig. 4. (a) Densifications of Cu-Y$_2$O$_3$ and CuCrZr-Y$_2$O$_3$ and (b) hardness for non irradiated sample values as a function of vol. % of Y$_2$O$_3$.

grit to minimize subsurface microcracking. In order to investigate the flexural strength of these novel high entropy alloys in their expected operating temperature range, TPB tests were performed at 200, 400, and 600 °C under a high vacuum atmosphere (10^{-6} mBar). The heating rate was 30 °C/min and, once the set point was reached, the heating was held for 10 min for the thermal stabilisation of the system before testing. Euler-Bernoulli equations later computed flexural strength for slender beams up to failure on the average of at least three measurements.

3. Results and discussion

Fig. 1 shows the microstructures of Cu-Y$_2$O$_3$ and CuCrZr-Y$_2$O$_3$ samples with 1, 5, and 10 vol% of Y$_2$O$_3$. All the consolidated materials consisted of Y$_2$O$_3$ particles dispersed in a Cu or CuCrZr matrix where some Y$_2$O$_3$ agglomerates can be distinguished. The Y$_2$O$_3$ particles are homogeneously distributed in the material, with no preferential location, and the presence of Cu oxides was identified (Fig. 1(a)) in samples with a Cu matrix. Fig. 2 evidences the EDS map of the sample 95Cu-5Y$_2$O$_3$, where particles of copper oxide can be identified at the grain boundaries. These oxides were not identified in the 95CuCrZr-5Y$_2$O$_3$. In fact, the presence of such oxides is unavoidable, even using an N$_2$

atmosphere, since copper powder surface tends to form a small number of oxides [22]. Moreover, low temperature sintering is associated with the surface diffusion process, while high temperature point to a grain bondary diffusion. In fact, both pehnonmena are recognized on the microstructure associated with a high compacting pressure which creates a more intense effect of the diffusion process ensuring low porosity. The existence of such copper oxide particles at the grain boundaries can promotes residual stresses on the material which can influence the mechanical performance.

Fig. 3 shows the microstructure of the irradiated 95Cu-5Y$_2$O$_3$ and 95Cu-5Y$_2$O$_3$ samples. No severe changes were observed on the surface of the samples. In fact, the materials showed irradiation resistance when submitted to the Ar$^+$ ions.

Fig. 4(a) evidences the values of densification for all the Cu-Y$_2$O$_3$ an CuCrZr-Y$_2$O$_3$ samples as a function of volume % of Y$_2$O$_3$. The increase in yttrium oxide particles promotes the agglomeration of the particles lowering their distribution in the grain boundary, resulting in a decrease in the density of the materials [3,24]. In addition, CuCrZr samples presented lower densification values compared with those of Cu. The hardness measurements applying 20N load for all the non irradiated samples are shown in Fig. 4(b). For all compositions, hardness values are
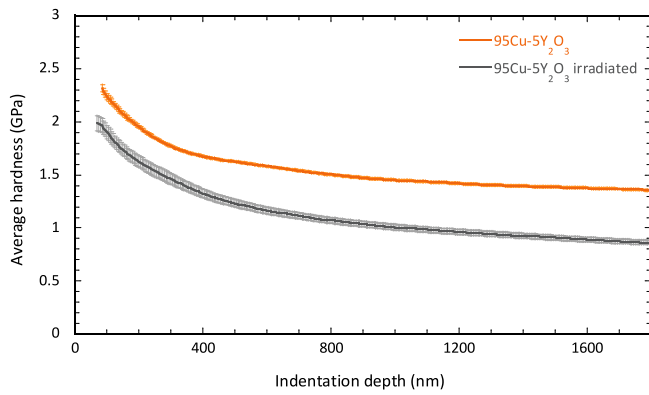
Fig. 5. Averaged nanoindentation curves for hardness of 95Cu-5Y₂O₃, unirradiated and Ar irradiated.

Fig. 6. Thermal conductivity for the samples with pure Cu [30], pure CuCrZr, 95CuCrZr-5Y₂O₃, 95Cu-5Y₂O₃, and pure W [29].

similar for Cu and CuCrZr-Y$_2$O$_3$ matrix samples. Note that the CuCrZr composite has a small quantity of Cr and Zr (99.11Cu-0.85Cr-0.04Zr nominal composition), which influences not substantially the hardness.

Moreover, the dispersion of yttria in a copper matrix shows considerable hardness enhancement compared to pure copper (35–37 HV) [23]. In fact, the same situation was verified for CuCrZr, one alloy without any thermal treatment and with the composition 98.9CuCrZr-1Cr-0.1Zr evidence of a value of 60 HV [24]. The addition of Y$_2$O$_3$ particles prevents the copper grain from growing without restrictions, thus maintaining the grain size. Therefore, the results established that the hardness is increased by adding the volume percentage of yttria in the composites, since the hard particles act as a barrier for indenter penetration through the matrix, which is related with the accumulations of the dislocations on the deformed zone. To evaluate the change in the mechanical properties due to the Ar irradiation, the CSM nanoindentation technique was used. It is well known that the elastic properties are less sensitive to irradiation damage than plastic properties such as hardness and yield stress, thus only hardness has been evaluated for irradiated and unirradiated 95Cu-5Y$_2$O$_3$ specimens. The plot in Fig. 5 shows the results of the hardness plus standard error with the indentation depth. Values below 80 nm are omitted due to surface testing artefacts.

For both samples, a decrease in hardness with an increase in indent depth was observed. Such depth-dependent hardness behaviour has been noticed as an indentation size effect (ISE) [25] furthermore, the deviations are larger at shallower depths, as expected, and asymptotically approaching the values 1.58 and 1.20 GPa, for unirradiated and irradiated specimens, respectively, as the depth of indentation increased. Considering the small penetration depth of the argon ions of about 200 nm, indentation tests will always probe additional unaffected material below the affected layer, thus not reflecting only the hardness of the affected layer. However, the trend of softening through argon irradiation is clear and is maintained at all indentation depths. The decrease in hardness observed after irradiation can arise from several sources, including recrystallisation/annealing, swelling of the voids, and relaxation of residual stresses. Although irradiation-enhanced recrystallization may explain a part of the decrease in hardness [26], the nucleation of voids in vacancy clusters seems to be the main factor influencing the mechanical properties. This effect has previously been addressed by other authors [27–29] when Cu-based materials were irradiated at large fluences, although the size and density of these voids depend on the grain size and irradiation temperature. As indicated in [27], irradiation hardening is the dominant mechanism at low irradiation fluences, since hardness critically depends on ease of dislocation motion, irradiation-induced point defects act as obstacles to dislocations motion. However, with the considerably high ion fluence selected in this work (1x10^{19} ions/cm^2 to peak levels of 100 dpa), the softening of void swelling and the development of a compressive residual stress state all
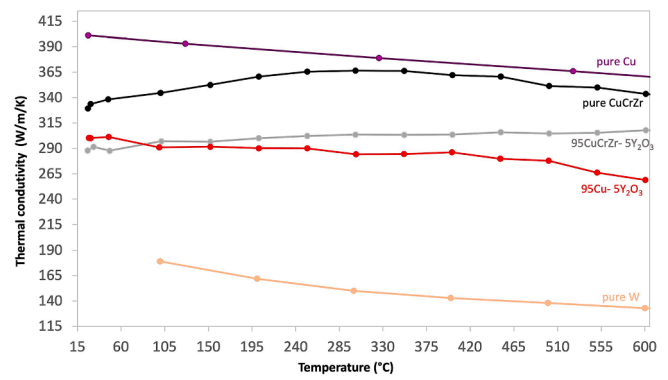
influence the measured hardness, although further experiments are needed to separate the influence of each defect to provide a better understanding. In this context, Gigax et al. [30] performed microshear test experiments on Cu irradiated Cu to a dose of 110 dpa and observed considerable softening of the material due to large void swelling values (~20%).

A thermal barrier between the W plasma facing component and the CuCrZr heat sink should have low thermal conductivity (10–15 W/m/k) to guarantee a heat flux of about 10 MW/m^2 [13,31,32]. Since the densification of the samples with a higher volume of Y$_2$O$_3$ presented a lower densification, only one sample with high densification was chosen to be studied (with 5 vol% of Y$_2$O$_3$). Fig. 6 shows the thermal conductivity for the samples 95CuCrZr-5Y$_2$O$_3$, and 95Cu-5Y$_2$O$_3$, pure CuCrZr, W [33], and Cu [34]. The thermal conductivity values for all the samples measured are lower than pure Cu and higher than pure W. Moreover, the results show that the thermal conductivity decreases when the volume % of yttria increases. Therefore, the presence of yttria oxide significantly impacts thermal properties, reducing thermal conductivity. As the samples were prepared from Cu powders, they may contain a residual oxygen level and this may also contribute for that reduction. Finally, for the same volume % of Y$_2$O$_3$, the composites with a CuCrZr matrix have slightly higher values than the ones with Cu. This may be rationalized considering that both Cr and Zr may combine with the residual oxygen present during consolidation hence producing a "cleaner" higher conductivity matrix. For CuCrZr, the low conductivity is generated by the combination of low Y$_2$O$_3$ percentage and low quantities of Cr (and Zr) in a solid solution. For CuCrZr, the low conductivity is generated by the combination of low Y$_2$O$_3$ percentage and low quantities of Cr (and Zr) in a solid solution. Based on the goal proposed for the thermal conductivities for the thermal barriers for the divertor (15 W/m/k [31]) it is possible to conclue that the present composites with these volme % of ytria are not adequated for this application. However, in fact, the addition of yttria oxide (about 40 % volume) to Cu generates a considerable change in thermal properties [13].

Fig. 7 displays the 95Cu-5Y$_2$O$_3$ and 95CuCrZr-5Y$_2$O$_3$ stress–strain curves for different temperatures (25, 400, and 600 °C). A ductile behavior was observed for all the compositions and temperatures. The 95CuCrZr- 5Y$_2$O$_3$ samples, exhibits six-fold increase in Ultimate Tensile Stress (UTS) at 600 °C when compared to that of 95Cu-5Y$_2$O$_3$. However, this difference was lower as the temperature decreased. Table 3 shows the yield stress and UTS values extracted from Fig. 7.

The mechanical properties for CuCrZr - IG Alloy seamless tubes for the ITER divertor [35] should have yield stress around 240 e 200 MPa and a UTS of 370 and 280 MPa for 20 °C and 250 °C, respectively. Comparing these values with the ones exhibited by the Y$_2$O$_3$ composites shows that CuCrZr-5Y$_2$O$_3$ alloy presents a considerable increase in UTS, and its mechanical properties at higher temperatures are significantly better than those of copper composite. The flexural strength as function
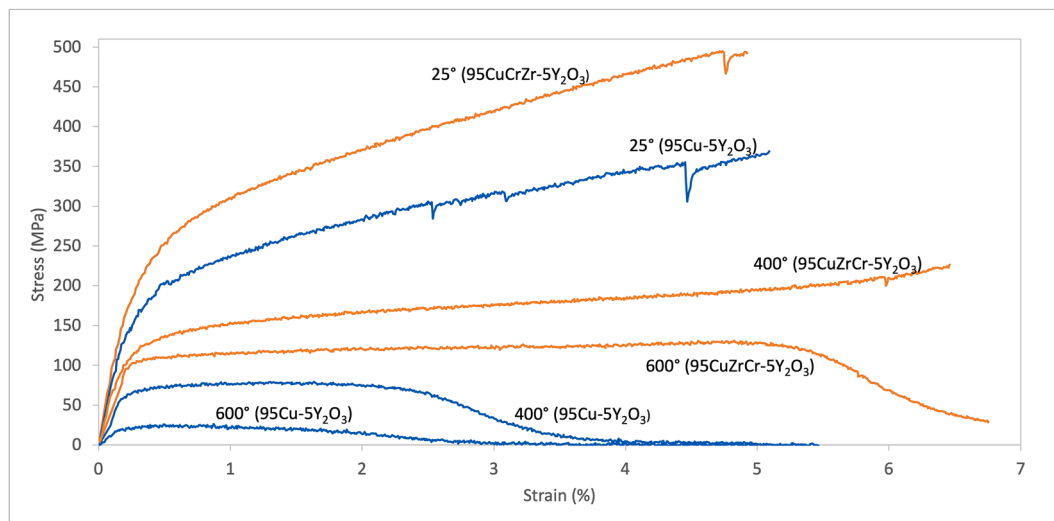
Fig. 7. Stress-Strain curve for 95Cu-5Y$_2$O$_3$ and 95CuCrZr-5Y$_2$O$_3$ at 25 °C, 400 °C, and 600 °C.

Table 3
Yield Stress and UTS experimental values for 95Cu-5Y$_2$O$_3$ and 95CuCrZr-5Y$_2$O$_3$ samples.

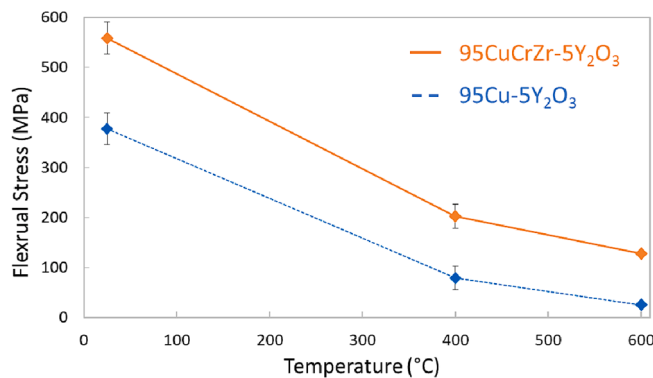| Samples(%v/v)	Experimental Conditions		
	Temperature (°C)	Yield Stress MPa	UTS MPa
95Cu-5Y$_2$O$_3$	25	150	369
	400	55	79
	600	16	25
95CuCrZr-5Y$_2$O$_3$	25	168	494
	400	121	226
	600	102	130

Fig. 8. Flexural strength as a function of temperature measured for Cu-5Y$_2$O$_3$ and CuCrZr-5Y$_2$O$_3$.

of temperature is shown in Fig. 8. It is possible to observe that the flexural strength obtained in Cu-5Y$_2$O$_3$ is lower than CuCrZr-5Y$_2$O$_3$; nevertheless, both samples present the same behavior with the temperature where the flexural strength decreases with it.

4. Conclusions

The Cu-Y$_2$O$_3$ and CuCrZr-Y$_2$O$_3$ composites were prepared in a glove box and consolidated with spark plasma sintering to be used as thermal barriers. The samples were produced with Cu and CuCrZr matrices and changed the volume fraction of Y$_2$O$_3$ (1, 5, and 10 vol%). The microstructures show the dispersions of Y$_2$O$_3$ regions in the Cu matrix and CuCrZr with the presence Y$_2$O$_3$, and the densifications achieved are between 90 and 98 %, which decrease with the increase of Y$_2$O$_3$ volume content. Furthermore, although the Ar irradiation of the samples with higher densification (95Cu-Y$_2$O$_3$ and 95CuCrZr-5Y$_2$O$_3$) did not show surface modification, nanoindentation testing resulted in a reduction of hardness with irradiation, this was due to foam-like behaviour arising from nucleation of voids at vacancy clusters. The thermal conductivities found for the 95Cu-Y$_2$O$_3$ and 95CuCrZr-5Y$_2$O$_3$ samples were higher than the desired values for thermal barriers in nuclear fusion reactors. All the samples presented a ductile behavior at the studied temperatures.

Declaration of Competing Interest

The authors declare that they have no known competing financial interests or personal relationships that could have appeared to influence the work reported in this paper.

References

[1] J. Blair, M.G. Lacy, Inelatic response of woven carbon/copper composite, Part 1: Experimental characterization, Ann. Am. Acad. Pol. Soc. Sci. 503 (1) (1993) 122–136.
[2] N. Tran, C.C. Wang, Optimization of the airside thermal performance of mini-channel-flat-tube radiators by using composite straight-and-louvered fins, Int. J. Heat Mass Transf. 160 (2020), 120163.
[3] Z. Mu, H.R. Geng, M.M. Li, G.L. Nie, J.F. Leng, Effects of Y2O3 on the property of copper based contact materials, Compos. Part B Eng. 52 (2013) 51–55.
[4] S. Mallik, N. Ekere, C. Best, R. Bhatti, Investigation of thermal management materials for automotive electronic control units, Appl. Therm. Eng. 31 (2–3) (2011) 355–362.

[5] J.H. You, et al., European DEMO divertor target: Operational requirements and material-design interface, Nucl. Mater. Energy 9 (2016) 171–176.

[6] G. Celebi Efe, T. Yener, I. Altinsoy, M. Ipek, S. Zeytin, C. Bindal, The effect of sintering temperature on some properties of Cu-SiC composite, J. Alloys Compd. 509 (20) (2011) 6036–6042.

[7] A. Strojny-Nędza, K. Pietrzak, W. Węglewski, The influence of Al2O3 powder morphology on the properties of Cu-Al2O3 composites designed for functionally graded materials (FGM), J. Mater. Eng. Perform. 25 (8) (2016) 3173–3184.

[8] M.A. Atwater, D. Roy, K.A. Darling, B.G. Butler, R.O. Scattergood, C.C. Koch, The thermal stability of nanocrystalline copper cryogenically milled with tungsten, Mater. Sci. Eng. A 558 (2012) 226–233.

[9] M. Al-Hajri, A. Melendez, R. Woods, T.S. Srivatsan, Influence of heat treatment on tensile response of an oxide dispersion strengthened copper, J. Alloys Compd. 290 (1–2) (1999) 290–297.

[10] M.S. Nagorka, C.G. Levi, G.E. Lucas, S.D. Ridder, The potential of rapid solidification in oxide-dispersion-strengthened copper alloy development, Mater. Sci. Eng. A 142 (2) (1991) 277–289.

[11] H. Zhuo, J. Tang, N. Ye, A novel approach for strengthening Cu-Y2O3 composites by in situ reaction at liquidus temperature, Mater. Sci. Eng. A 584 (2013) 1–6.

[12] K. Biswas, et al., High-performance bulk thermoelectrics with all-scale hierarchical architectures, Nature 489 (7416) (2012) 414–418.

[13] M. Galatanu, M. Enculescu, G. Ruiu, B. Popescu, A. Galatanu, Cu-based composites as thermal barrier materials in DEMO divertor components, Fusion Eng. Des. 124 (2017) 1131–1134.

[14] M. Galatanu, M. Enculescu, A. Galatanu, Thermophysical properties of Cu-ZrO2 composites as potential thermal barrier materials for a DEMO W-monoblock divertor, Fusion Eng. Design 127 (2018) 179–184.

[15] D.V. Kudashov, H. Baum, U. Martin, M. Heilmaier, H. Oettel, Microstructure and room temperature hardening of ultra-fine-grained oxide-dispersion strengthened copper prepared by cryomilling, Mater. Sci. Eng. A 387–389 (1–2 SPEC. ISS) (2004) 768–771.

[16] S.M.S. Aghamiri, et al., Microstructure and mechanical properties of mechanically alloyed ODS copper alloy for fusion material application, Nucl. Mater. Energy 15 (2018) 17–22.

[17] F. Huang, H. Wang, B. Yang, T. Liao, Z. Wang, Uniformly dispersed Y 2 O 3 nanoparticles in nanocrystalline copper matrix via multi-step ball milling and reduction process, Mater. Lett. 242 (2019) 119–122.

[18] G.L. Kulcinski, A.B. Wittkower, G. Ryding, Use of heavy ions from a tandem accelerator to simulate high fluence, fast neutron damage in metals, Nucl. Instrum. Methods 94 (2) (1971) 365–375.

[19] G.S. Was, Challenges to the use of ion irradiation for emulating reactor irradiation, J. Mater. Res. 30 (9) (May 2015) 1158–1182.

[20] M. R. Gilbert, S. L. Dudarev, D. Nguyen-Manh, S. Zheng, L. W. Packer, J.-C. Sublet, Neutron-induced dpa, transmutations, gas production, and helium embrittlement of fusion materials, (2013).

[21] W.C. Oliver, G.M. Pharr, An improved technique for determining hardness and elastic modulus using load and displacement sensing indentation experiments, J. Mater. Res. 7 (6) (1992) 1564–1583.

[22] F. Huang, H. Wang, J.S. Chen, B. Yang, Dry ball milling and wet ball milling for fabricating copper–yttria composites, Rare Met. 37 (10) (2018) 859–867.

[23] J. Naser, W. Riehemann, H. Ferkel, Dispersion hardening of metals by nanoscaled ceramic powders, Mater. Sci. Eng. A 234–236 (1997) 467–469.

[24] A. Brotzu, F. Felli, D. Pilone, V. Di Cocco, G. Sindoni, I. Ciufolini, Study of CuCrZr alloy for the production of a passive satellite, Procedia Struct. Integr. 18 (2019) 742–748.

[25] W.D. Nix, H. Gao, Indentation size effects in crystalline materials: A law for strain gradient plasticity, J. Mech. Phys. Solids 46 (3) (1998) 411–425.

[26] S. J. Zinkle, A brief review of cavity swelling and hardening in irradiated copper and copper alloys.

[27] S. Zhang, B. Shi, J. Wang, P. Jin, Stress-induced gradient rejuvenation framework and memory effect in a metallic glass, Scr. Mater. 213 (2022), 114636.

[28] M. Hatakeyama, H. Watanabe, M. Akiba, N. Yoshida, Low void swelling in dispersion strengthened copper alloys under single-ion irradiation, J. Nucl. Mater. 307–311 (2002) 444–449.

[29] M. Mohammadreza Seyedhabashi, M. A. Tafreshi, B. Shirani bidabadi, S. Shafiei, A. Abdisaray, Damage study of irradiated tungsten and copper using proton and argon ions of a plasma focus device," Appl. Radiat. Isot., 154 (2019) 108875.

[30] J.G. Gigax, et al., A novel microshear geometry for exploring the influence of void swelling on the mechanical properties induced by MeV heavy ion irradiation, Materials (Basel) 15 (12) (2022) 4253.

[31] T.R. Barrett, et al., Enhancing the DEMO divertor target by interlayer engineering, Fusion Eng. Design 98–99 (2015) 1216–1220.

[32] V. International Atomic Energy Agency, "ITER. EDA Documentation Series No. 24 International," p. 816, 2002.

[33] M. Fukuda, A. Hasegawa, S. Nogami, Thermal properties of pure tungsten and its alloys for fusion applications, Fusion Eng. Des., 132(2017) (2018) 1–6.

[34] eFunda.Inc, "Copper Thermal Conductivity," 1999.

[35] ITER, Material Specification for the supply of CuCrZr - IG alloy seamless tubes for the ITER divertor.